On the Use of Energy Storage Systems and Linear Feedback Optimal Control for Transient Stability

Abdallah Farraj, *Member, IEEE*, Eman Hammad, *Student Member, IEEE*, and Deepa Kundur, *Fellow, IEEE*

***Abstract*—In this paper, we study a distributed control strategy that harnesses the highly granular data available in future power systems in order to improve system resilience to disturbances. Specifically, we investigate the role of external energy storage systems (ESSs) in stabilizing the dynamics of power systems during periods of disruption. We consider an information-rich multiagent framework and focus on ESS output control via linear feedback optimal (LFO) control to achieve transient stability. The LFO control scheme relies on receiving timely state information to actuate distributed ESSs in order to drive the synchronous generators to stability. We evaluate the performance of the LFO control on the 39-bus 10-generator New England test power system in the presence of ideal and nonideal conditions including communication latency, finite sampling rate, and sensor noise. The LFO controller is found to have a simple structure, be tunable, and to have fast response to achieving transient stability while being sensitive to information latency and data rate.**

***Index Terms*—Cyber–physical agents, distributed control schemes, energy storage systems (ESSs), feedback design, optimal control, smart grid, system resilience, transient stability.**

I. Introduction

SMART grids are enjoying a recent interest from both academic and industrial communities [1], [2]. Such systems improve the resilience and efficiency of power delivery systems by employing advanced control, communications, and analytics [3]–[5]. Smart grid systems also facilitate the integration of renewable resources and distributed storage. Recent economical, technical, and environmental factors have motivated growth in small-scale external energy storage systems (ESSs) that include both distributed generation and storage units. The integration of ESSs into power systems requires the study of appropriate distributed control methodologies.

Manuscript received July 13, 2016; revised September 19, 2016; accepted November 18, 2016. Date of publication November 24, 2016; date of current version August 1, 2017. Paper no. TII-16-0703. *(Corresponding author: A. Farraj.)*

The authors are with the Department of Electrical and Computer Engineering, University of Toronto, Toronto, ON M5S 3G4, Canada (e-mail: abdallah@ece.utoronto.ca; ehammad@ece.utoronto.ca; dkundur@ece.utoronto.ca).

Color versions of one or more of the figures in this paper are available online at http://ieeexplore.ieee.org.

Digital Object Identifier 10.1109/TII.2016.2632760

Significant opportunities exist for the development of advanced control schemes due to the availability of rich and highly granular information on the state of the power grid components [6]. The use of advanced telemetry and communications technologies promotes new opportunities to design and implement nontraditional control strategies; through mitigating certain forms of cyber and physical disturbances, such control schemes can enhance the resilience and operation of power systems. Therefore, new distributed control schemes that take advantage of the volume of data and that can simultaneously harvest the availability of ESSs are of timely value to smart grid system designers. As such, recent research has focused, in part, on cyber-enabled control schemes that utilize external power sources [7]–[10]. The concept of flocking is employed in [8] for distributed control that addresses transient stability of synchronous generators under severe disturbance. More recently, a feedback linearization-based distributed control strategy is proposed in [10] to stabilize the grid after a physical or cyber disturbance. Furthermore, sliding-mode control paradigms are considered in [11]–[13], and a game-theoretic approach for stability during switching attacks are employed in [14] and [15]. These control schemes all exhibit complex nonlinear designs. In addition, it can be observed that flocking-based controllers are slow to converge. Thus, it is critical to investigate aggressive yet computationally simpler methods for transient stabilization.

In this paper, we investigate the application of optimal control in a smart grid setting. We use a multiagent framework model to facilitate modeling of different cyber–physical interactions and studies of system behavior. The resulting insights complement contributions of the power control community by considering nontraditional control schemes that harvest the capabilities of the ESSs and take advantage of the rich communication environment in smart grids. To investigate cyber–physical dependencies within a tractable paradigm, we focus in this paper on the problem of synchronous generators' transient stability. As such, the scope of this paper is to investigate the application and performance of optimal control schemes that rely on distributed ESS for transient stability studies. Other relevant issues including small-signal stability, voltage stability, and control of nonsynchronous generators are beyond the scope of this paper, and serve as complementary control strategies to the proposed paradigm.

Optimal linear control has been traditionally considered in the context of an ideal environment, where the limitations on

information availability and integrity make it challenging to implement [16]. Motivated by the promise of a resource-rich future power grid, we explore optimal linear control of ESSs to address transient stability. The analysis problem is more tractable and computationally cheaper as the controller is linear. Specifically, the control signal is calculated using a linearized version of the swing equation model.

Linear feedback optimal (LFO) control aims to minimize an associated cost function based on system state information in order to stabilize the rotor speed of synchronous generators after the onset of transient instability. Distributed controllers receive frequent sensor measurements that are transmitted through the communication network. In response to a disturbance, the LFO controllers actuate change in the power system through power injection and absorption via ESSs that are proximal to the synchronous generators. The actuation process stabilizes the power system by minimizing the difference between the system state variables and their optimal values.

Thus, in this paper, we:

1) investigate the distributed control problem for a typical transmission system leveraging the cyber–physical opportunities in smart grid infrastructure;
2) develop, apply, and evaluate linear quadratic optimal control theory in the context of a distributed control framework for transient stability in a multiagent smart grid setting; optimal control was formerly considered infeasible in power systems due to the lack of communication infrastructure and measurement;
3) evaluate controller performance under practical measurement and communication constraints to assess the practical value of the proposed work; and
4) compare the performance of the LFO controller to four recently published approaches to draw insights on the potential value of the controller as a compensation strategy complementary to traditional approaches.

We investigate linear optimal feedback control because of the following reasons.

1) Recent works employ nonlinear control schemes; however, less work investigates the application of a distributed linear control scheme.
2) With the higher communication connectivity in smart grids, the implementation of linear optimal feedback control schemes can become feasible.
3) The distributed nature of the controller is possible due, partially, to the increased installations of renewable energy sources and storage devices.
4) It has a comparable, if not better, performance with other recently published nonlinear controllers.
5) It has a cost advantage over the nonlinear ones given that its structure is simpler.

The remainder of this paper is organized as follows. The proposed work is placed in context to traditional power system stability strategies in Section II. The problem setup is presented in Section III. The LFO control scheme is developed in Section IV. Section V numerically investigates the performance of the developed controller. Final remarks and conclusions are provided in Section VI.

II. Power System Stability Studies

The main contribution of this paper focuses on the use of distributed ESS and optimal control to achieve transient stability. In this section, we briefly overview other forms of stability and associated best practices to provide perspective to our contributions and its scope. We emphasize that our approach leverages the cyber-enabled trend of smart grid systems and represents an emerging compensation strategy complementary to and in support of those traditional forms that we discuss in this section.

A. Power System Stability

Power system stability is traditionally defined as the ability of the system to regain a state of operating equilibrium after being subjected to a physical disturbance [17]. Classically, power system disturbances considered in system studies have been physical in nature. Typically, such disturbances have been classified as either "small" or "large" [17], whereby examples of small and large disturbances include incremental load changes and transmission line faults, respectively. As power systems mature into smart grid entities, we observe burgeoning classes of cyber failures and attacks that can fall within the small or large classes of disturbances depending on their degree of impact. As a result, stability studies are more recently including both cyber and physical contingencies.

As well accepted, stability studies are categorized based on time span (short term or long term) or disturbance size (small or large). Moreover, system stability is classified into rotor angle stability, voltage stability, and frequency stability [17]. The particular stability class considered depends on the observed system variables under consideration in the study. Typically, stability studies related to these three classes are complementary, hence advances in all aspects of stability will benefit the power system operation.

1) Voltage Stability: Voltage stability enables the maintenance of voltage levels (within a given range) at all buses in the presence of a disturbance. Instability in voltage can have the effect of tripping power system components leading to cascading outages with high negative impact. It is well known that voltage stability depends on the ability of the power system to maintain or restore equilibrium between power demand and supply at the load buses. In practice, a common criterion used to assess voltage stability involves studying the capability of the power system to supply its load with reactive power for a given demand of real power [18]; specific metrics used include critical load demand before a voltage collapse, $V - Q$ sensitivity analysis, and voltage stability indices.

Traditionally, voltage instability is addressed by reinforcing the power system through installing series compensation and shunt capacitor banks on the transmission line. Flexible alternating current transmission systems (FACTS) devices are also employed to control the voltage levels. FACTS devices are used to enhance system performance and controllability and are mainly based on power electronics. For example, a static VAR compensator or a static synchronous compensator (STATCOM) can inject current in the power system to improve the voltage stability.

FACTS devices can provide greater control of power transfer, prevent cascading outages, and damp system oscillations [19].

2) Frequency Stability: The ability of a power system to maintain steady frequency following a disturbance is called frequency stability [17]; stabilizing frequency depends on the ability of the system to maintain or restore equilibrium between power generation and load. As commonly observed, frequency instability appears in the form of sustained frequency swings that leads to tripping of generators or loads. In large interconnected power systems, this type of instability is most commonly associated with conditions following splitting of systems into islands [17].

Traditionally, the governor control maintains the frequency of the electrical signal by controlling the input mechanical power of the synchronous generator. The input mechanical power is slowly varied depending on the frequency value using a speed–droop curve. Primary, secondary, and tertiary types of control can be overlapped to restore the frequency. Defense mechanisms against frequency instability include controlled load shedding or generation unit tripping [18].

Furthermore, the automatic voltage regulator (AVR) is used by the excitation controller to maintain the magnitude of the terminal voltage of a synchronous generator within a specified level. Specifically, the terminal voltage is measured and, after filtering, is compared with a reference voltage; the resulting error signal is amplified and fed to the excitation controller, which consequently affects the generator's field current. If the terminal voltage drops below an acceptable threshold, the excitation system increases the field current to increase the output reactive power in order to increase the terminal voltage [20].

3) Rotor Angle Stability: This stability refers to the ability of the synchronous machines in a power system to remain in synchronism after being subjected to a disturbance [21], and it depends on the ability of a synchronous generator to maintain or restore balance between its electromagnetic and mechanical torques. A balance between mechanical and electromagnetic torques results in constant rotor speed, which results in normal operation of the power system. An imbalance results in acceleration or deceleration of rotor speed depending on the sign and magnitude of the torque difference.

Small-signal rotor angle stability studies the ability of the power system to maintain synchronism when subjected to small disturbances. Usually, the time frame of these studies is on the order of 10–20 s following the small disturbance. A power system stabilizer (PSS) is a power controller that is often used to damp out oscillations. PSS affects the input signal of the AVR to enhance the terminal voltage and overall system stability. A typical PSS includes a gain block to determine the amount of damping, a Washout block to filter the rotor speed oscillations, and a phase-compensation block to compensate for the phase lag between the AVR input and the generator electrical torque [22], [23].

Transient stability is concerned with the ability of the power system to maintain synchronism when subjected to severe disturbance. The time frame of these studies is usually 3–5 s following the disturbance, and it may extend to 10–20 s for very large power systems [17].

B. Transient Stability

Transient stability requires maintaining both rotor phase angle cohesiveness and exponential rotor speed synchronization after the occurrence of a disturbance. Phase angle cohesiveness refers to the property whereby the absolute differences between the rotor phase angle of the different synchronous generators are below a predefined threshold. Exponential speed synchronization requires the rotor speed of the generators to converge asymptotically to a common value. Through possible application of control strategies, transient stability can be achieved and/or enhanced.

We employ a swing equation model to describe the changing dynamics of the synchronous generators in a power system. Specifically, the swing equation links the rotor speed and angle that enables the study of transient stability. A Kron-reduction technique [24] is employed to efficiently reduce the modeling of power grid interconnections and determine effective mutual couplings. In conjunction with the swing equation model of each generator, an overall system of coupled differential equations can be employed to represent the overall transient stability dynamical behavior of the power system.

Let the number of synchronous generators in the power grid be denoted as N. Furthermore, for Generator i, where $i \in \{1, \ldots, N\}$, E_i denotes the generator's internal voltage [in per unit (p.u.)], $P_{e,i}$ represents its electrical power (in p.u.), $P_{m,i}$ denotes its mechanical power (in p.u.), ω_i refers to its relative normalized rotor speed (in p.u.), X'_{di} is its direct-axis transient reactance (in p.u.), δ_i represents its rotor angle (in radians), M_i refers to its inertia (in seconds), and D_i denotes its damping coefficient (in seconds). The relative normalized rotor speed of Generator i $\forall i \in \{1, \ldots, N\}$ is defined as $\omega_i = \left(\omega_i^{\text{act}} - \omega^{\text{nom}}\right)/\omega^{\text{nom}}$, where ω^{nom} is the nominal angular speed (in radians per second) of the power system and ω_i^{act} is the actual angular rotor speed of Generator i. Furthermore, $P_{a,i} = P_{m,i} - P_{e,i}$ denotes the accelerating power of Generator i.

Let $\dot{\delta}_i$ and $\dot{\omega}_i$ denote the derivatives of δ_i and ω_i with respect to time, respectively. The swing equation of Generator i is expressed as [22]

$$\begin{aligned} \dot{\delta}_i &= \omega_i \\ \dot{\omega}_i &= \frac{1}{M_i}\left(-D_i\,\omega_i + P_{a,i}\right). \end{aligned} \tag{1}$$

Furthermore, $P_{e,i}$ is calculated as [25]

$$P_{e,i} = \sum_{k=1}^{N} |E_i||E_k|\left(G_{\text{ik}}\cos\left(\delta_i - \delta_k\right) + B_{\text{ik}}\sin\left(\delta_i - \delta_k\right)\right) \tag{2}$$

where $G_{\text{ik}} = G_{\text{ki}} \geq 0$ is the Kron-reduced equivalent conductance between Generator i and Generator k, and $B_{\text{ik}} = B_{\text{ki}} t > 0$ is the Kron-reduced equivalent susceptance between Generator i and Generator k $\forall i, k \in \{1, \ldots, N\}$.

Define $\boldsymbol{\omega} = [\omega_1, \cdots, \omega_N]^T$ and $\boldsymbol{\delta} = [\delta_1, \cdots, \delta_N]^T$, and let $\boldsymbol{x} = [\boldsymbol{\delta}, \boldsymbol{\omega}]^T$ denote the state variable of the power system. Also,

define

$$\boldsymbol{P}_m = [P_{m,1}, \cdots, P_{m,N}]^T, \boldsymbol{D} = \text{diag}(D_1, \ldots, D_N)$$
$$\boldsymbol{P}_e = [P_{e,1}, \cdots, P_{e,N}]^T, \boldsymbol{M} = \text{diag}(M_1, \ldots, M_N). \quad (3)$$

Furthermore, let $\boldsymbol{P}_a = \boldsymbol{P}_m - \boldsymbol{P}_e$. It is to be noted that $\boldsymbol{P}_a$ is a function of $\boldsymbol{x}$ because $\boldsymbol{P}_e$ is a function of $\boldsymbol{x}$, as shown in (2). Consequently, the vector swing equation is shown to be

$$\dot{\boldsymbol{x}} = \begin{bmatrix} \boldsymbol{0}_{N\times N} & \boldsymbol{I}_{N\times N} \\ \boldsymbol{0}_{N\times N} & -\boldsymbol{M}^{-1}\boldsymbol{D} \end{bmatrix} \boldsymbol{x} + \boldsymbol{M}^{-1}\boldsymbol{P}_a. \quad (4)$$

Transient stability is traditionally evaluated by studying circuit breakers' critical clearing time [23]. It is also assessed by studying transient energy functions based on Lyapunov's method and equal area criterion. Furthermore, boundary controlling unstable equilibrium points and potential energy boundary surface are widely used in multimachine power systems [23, Ch. 9]. Classical approaches for transient stability control include the use of fast-acting circuit breakers to trip the faulted transmission lines in order to clear the fault, using automatic power control regulators to affect the excitation and governor systems of a synchronous generator, and employing out-of-step protection systems [18].

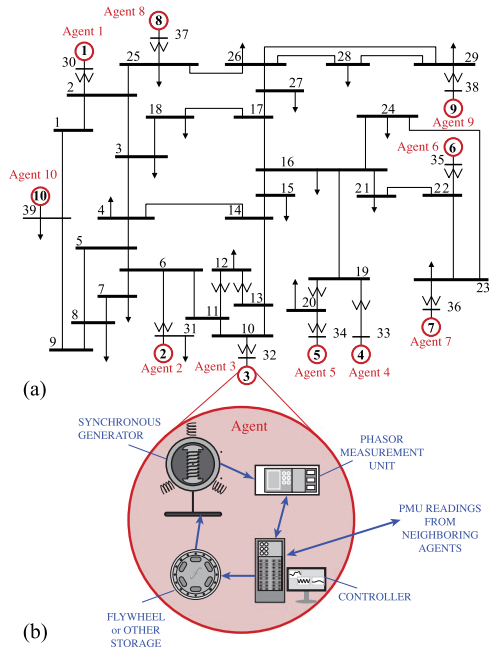

Fig. 1. Multiagent framework for smart grid systems. (a) New England test power system. (b) Sample cyber–physical agent.

III. Distributed Control for Transient Stability

In this paper, we focus on leveraging the growing penetration of fast acting distributed storage and the increased communication connectivity in power systems and propose a multiagent distributed control paradigm for transient stability in emerging smart grid systems.

A. Multiagent Framework

An *agent* is defined as an autonomous entity that employs sensors and acts upon an environment using actuators to achieve specific goals. As intelligence is embedded within emerging smart grid devices, modeling such components as agents is gaining popularity in the technical community. To capture the behavior of interacting agents, a multiagent system paradigm is typically employed. Our Kron-reduced swing equation model of (4) represents an archetypal form of multiagent dynamical system in which the interactions amongst synchronous generators are modeled through a system of dynamical ordinary differential equations with state variables representing each generator rotor angle and speed.

As such, our multiagent framework employs an agent to represent a "smart" synchronous generator. Specifically, each agent consists of a local sensor that provides measurements of rotor angle and speed, a distributed controller that processes sensor data from the different agents of the power system, an ESS (such as a flywheel) that can inject or absorb real power in the power system in proportion to the value of the control signal, and a traditional synchronous generator. In this framework, a communication network connects the sensors and distributed controllers [26], [27]. For example, consider the New England 10-generator 39-bus test power system shown in Fig. 1 with the associated (cyber) infrastructure.

This framework naturally lends itself to a cyber–physical representation useful for studying distributed control that lies at the cyber–physical interface. The cyber component of the smart grid includes the distributed controllers, sensors, and communication infrastructure. In addition, the physical elements of the smart grid comprise the distributed ESSs, synchronous generators, and other associated power system devices. In this framework, the sensors represent the physical-to-cyber interface as they measure the required physical quantities and convert them to digital measurements. As an example, a phasor measurements unit (PMU) can be used to measure voltage and current readings from specific location in the power grid and send the time-stamped readings to phasor data concentrators. The sensors utilize the communication network to send the measurements to the controllers. Furthermore, the intersection between the distributed controllers and the ESSs represents the cyber-to-physical interface; the controllers take advantage of the cyber data to make change in the physical system through actuating the ESSs. In this model, physical coupling occurs between the cyber–physical agents through the transmission lines and cyber coupling happens because of the cyber-enabled control.

The reader should note that within this framework, we envision a reasonable penetration of ESSs (renewable and nonrenewable) and storage devices, which naturally enables the study of distributed ESS control. Specifically, we focus on a paradigm whereby an ESS is available at each generator bus. Practically, we relate the capacity of a certain ESS as a percentage of its associated synchronous generator power.

B. Distributed ESS and Transient Stability Control

While a multiagent control framework can be employed to model distributed control in a variety of contexts, our focus

is on transient stability employing distributed ESSs. In practice, different control schemes (such as excitation and governor control systems) accompany the synchronous generators in order to respond to different disturbances; however, such traditional control systems exhibit slow reaction to rapid changes in the system state. Moreover, circuit breaker protection may be insufficient for severe faults. Consequently, our distributed ESS framework provides an emerging paradigm to help achieve transient stability for a broader class of failures.

Advanced distributed control requires the presence of communication infrastructure to transmit system state information. Hence, sensor readings are periodically communicated to the distributed controllers in this framework, and the controllers actuate change in the power system dynamics through power injection and absorption using the ESS at the synchronous generator bus. To incorporate ESS actuation at the bus of Generator i, we modify the associated swing equation model in (1) to employ a power injection/absorption term u_i as follows:

$$\begin{aligned} \dot{\delta}_i &= \omega_i \\ \dot{\omega}_i &= \frac{1}{M_i}\left(-D_i\,\omega_i + P_{a,i} + u_i\right). \end{aligned} \tag{5}$$

This modification models how the distributed controller affects the power system dynamics by absorbing or injection real power of a specified amount (via an ESS) at the designated generator. A positive (negative) value of u_i indicates that the ESS at Generator i injects (absorbs) power. Let $\boldsymbol{u} = [u_1, \cdots, u_N]^T$ be the control output vector.

C. Recent Related Work

In order to demonstrate the potential of our multiagent framework in enhancing transient stability, we compare its performance to four recently proposed distributed control methods within the same class. These four approaches along with the proposed paradigm share the following attributes. All methods:

1) represent recent contributions to be applied to smart grid systems;

2) require communication connectivity for information sharing;

3) rely on controlling distributed ESSs for stabilization; and

4) tackle the problem of stability of power systems from the generator's perspective.

In [7], Mercier *et al.* propose optimizing the operation and control of a battery-based ESS (BESS) in order to regulate the frequency of the power system. The control objective is to minimize the peak frequency deviation during and after disturbances. Let Δf denote the system frequency deviation (in p.u.); specifically, it is proposed that no control action is required if $|\Delta f|$ is within 0.001 p.u. (called the noncritical frequency window). However, if 0.001 p.u. $\leq |\Delta f| <$ 0.004 p.u., then the output of the BESS is made linearly dependent on Δf. Furthermore, if $|\Delta f| \geq$ 0.004 p.u., then the BESS is proposed to absorb or inject power in its full rated capacity [7].

In [8], Wei *et al.* propose flocking-based control scheme in order to achieve generators' synchronization after the occurrence of a severe disturbance in the system. The flocking-based control scheme introduces a control signal that shapes the power system dynamics to imitate stable flock of bird-like objects. Specifically, the dynamics exhibit flock centering, collision avoidance, and velocity matching [28]–[30]; flock centering and collision avoidance can achieve phase synchronization, while velocity matching provides speed stabilization needed for transient stability [8]. In this flocking-based model, the control input is calculated as [8]

$$\boldsymbol{u} = \boldsymbol{\Phi} - \boldsymbol{G\delta} - \boldsymbol{B\omega}\cdot\boldsymbol{D}_f - c(\boldsymbol{\delta} - \boldsymbol{\delta_0}). \tag{6}$$

Here, $\boldsymbol{\Phi} = [\Phi_1, \ldots, \Phi_N]^T$ and Φ_i is defined as

$$\Phi_i = \sum_{k=1, k\neq i}^{N} \int_{t_0}^{t} \rho(\delta_i - \delta_k)\,\mathrm{d}t \tag{7}$$

where t is the time when the control signal is calculated, t_0 is the time when control scheme is activated, c is a flock navigation term, and ρ is a control function; furthermore, $\boldsymbol{\delta}_0 = [\delta_{0_1}, \ldots, \delta_{0_N}]^T$ are the phase values calculated at t_0, $\boldsymbol{D}_f = [D_1, \ldots, D_N]^T$, and both $\boldsymbol{B}$ and $\boldsymbol{G}$ are cyber control matrices that are function of the power system.

In [31], Andreasson *et al.* propose a consensus proportional integral (CPI)-based control strategy for automatic frequency control, where the mechanical power of a synchronous generator is adjusted depending on the outcome of a two-level process. The generator's rotor speed is regulated against a reference speed in the first level, and the reference speed is updated at the second level to eliminate errors. The CPI-based control signal is calculated as [31]

$$\begin{aligned} u_i &= \alpha_c\left(\hat{\omega} - \omega_i\right) \\ \dot{\hat{\omega}} &= \beta_c\left(w^{\text{nom}} - \frac{1}{N}\sum_{j=1}^{N}\omega_j\right) \end{aligned} \tag{8}$$

where α_c and β_c are constants.

A parametric feedback linearization (PFL) control scheme is proposed in [10] and [32] to achieve transient stability of synchronous generators after the occurrence of disturbances. The PFL controller receives periodic sensor measurements to regulate the output of distributed ESSs. The goal of the PFL control is to balance the swing equation model of the synchronous generators in order to drive the associated rotor speed to stability. Let $\alpha_i \geq 0$, the PFL controller's output is defined for Generator i as [10]

$$u_i = -\left(P_{a,i} + \alpha_i\,\omega_i\right). \tag{9}$$

The reader should note that we do not consider the traditional forms of protection discussed in Section II for comparison as such approaches are complementary and the proposed work could be interpreted as enhancing their operation in the context of smart grid.

IV. System-Wide Optimal Control

The prior art of Section III-C demonstrates the trend in developing nonlinear complex controller designs. In fact, both flocking and CPI controllers exhibit longer times to achieve transient

stability. This motivates the proposed work that, in part, aims to achieve a more aggressive controller yet with simpler structure. To achieve this, we explore the potential of using optimal control with ESS as a fast and low-complexity alternative to the nonlinear control approaches. Furthermore, we aim for a tunable controller using a design parameter.

A. Linearized Swing Equation

To apply LFO control, we must linearize our system model. Here, the standard dc power flow approximation [33] is used to linearize the electrical power formula in (2). This type of linearization is particularly applicable to power transmission systems, the focus of our study [34]. The electrical power of Generator i can be approximated as

$$\begin{aligned} P_{e,i} &\overset{a}{\approx} \sum_{k=1}^{N} |E_i|\,|E_k| B_{\text{ik}} \sin\left(\delta_i - \delta_k\right) \\ &\overset{b}{\approx} \sum_{k=1}^{N} |E_i|\,|E_k|\, B_{\text{ik}} (\delta_i - \delta_k) \end{aligned} \tag{10}$$

where (a) assumes that the line resistance is negligible compared to the reactance in all Kron-reduced transmission lines, and (b) assumes that rotor angle differences $(\delta_i - \delta_k)$ are small between Generators i and k. Then, utilizing this approximation, $\dot{\omega}_i$ is represented as [35]

$$\dot{\omega}_i = \frac{1}{M_i}\left(-D_i\omega_i + P_{m,i} + \gamma_{i,i}\delta_i + \sum_{k=1}^{N}\gamma_{i,k}\delta_k + u_i\right) \tag{11}$$

where $\forall i, k \in \{1, \ldots, N\}$

$$\gamma_{i,k} = |E_i| \begin{cases} |E_k|\, B_{\text{ik}}, & k \neq i \\ -\sum\limits_{j=1}^{N} |E_j|\, B_{\text{ij}}, & k = i\,. \end{cases} \tag{12}$$

Furthermore, let

$$\boldsymbol{\gamma} = \begin{bmatrix} \gamma_{1,1} & \cdots & \gamma_{1,N} \\ \gamma_{2,1} & \cdots & \gamma_{2,N} \\ & \ddots & \\ \gamma_{N,1} & \cdots & \gamma_{N,N} \end{bmatrix}. \tag{13}$$

Then, assuming the linearized swing equation approximation of (10) and (11), the dynamics of the synchronous generators of the power system can consequently be described as

$$\dot{\boldsymbol{x}} = \boldsymbol{A}\boldsymbol{x} + \boldsymbol{c} + \boldsymbol{L}\tilde{\boldsymbol{u}} \tag{14}$$

where

$$\begin{aligned} &\boldsymbol{A} = \begin{bmatrix} \boldsymbol{0}_{N\times N} & \boldsymbol{I}_{N\times N} \\ \boldsymbol{M}^{-1}\boldsymbol{\gamma} & -\boldsymbol{M}^{-1}\boldsymbol{D} \end{bmatrix}, \boldsymbol{L} = \begin{bmatrix} \boldsymbol{0}_{N\times N} & \boldsymbol{0}_{N\times N} \\ \boldsymbol{0}_{N\times N} & \boldsymbol{I}_{N\times N} \end{bmatrix} \\ &\boldsymbol{c} = \begin{bmatrix} \boldsymbol{0}_{N\times 1} & \boldsymbol{M}^{-1}\boldsymbol{P}_m \end{bmatrix}^T, \quad \tilde{\boldsymbol{u}} = \begin{bmatrix} \boldsymbol{0}_{N\times 1} & \boldsymbol{M}^{-1}\boldsymbol{u} \end{bmatrix}^T. \end{aligned} \tag{15}$$

B. LFO Control Design

We define a quadratic cost function for minimization as [36]

$$J_x = \int_{t_0}^{\infty} \boldsymbol{\omega}(t)^T \boldsymbol{Q}_x \boldsymbol{\omega}(t) + \boldsymbol{u}(t)^T \boldsymbol{R}_x \boldsymbol{u}(t)\, \mathrm{d}t \tag{16}$$

where t_0 is the time when the LFO controller is activated, $\boldsymbol{Q}_x \in \mathbb{R}^{N\times N}$ is a positive semidefinite matrix, and $\boldsymbol{R}_x \in \mathbb{R}^{N\times N}$ is positive definite. Then, $\boldsymbol{\omega}(t)^T \boldsymbol{Q}_x \boldsymbol{\omega}(t) \geq 0$ represents the penalty at time t when $\boldsymbol{\omega}(t)$ deviates away from $\boldsymbol{0}$. Similarly, $\boldsymbol{u}(t)^T \boldsymbol{R}_x \boldsymbol{u}(t) > 0$ represents the control effort in regulating $\boldsymbol{\omega}(t)$ to $\boldsymbol{0}$.

For the development of the control signal, we assume that there are no physical limitations on the amount of power that can be injected or absorbed by the different ESSs in the system; this assumption is needed for the sake of analysis traceability. Nevertheless, in reality, the ESSs have relatively smaller capacity compared to the synchronous generators of the power system. As such, the capacity of an ESS can be expressed as a percentage (for example, 5%) of the mechanical power of the associated generator. However, the distributed controller can stabilize the power system faster as the ESS capacity becomes higher.

Building on the findings of appendix, the value of the LFO control signal is calculated as

$$\boldsymbol{u} = -\boldsymbol{M}\boldsymbol{R}_x^{-1}\left(\boldsymbol{P}_{2,1}\left(\boldsymbol{\delta} + \boldsymbol{\gamma}^{-1}\boldsymbol{P}_m\right) + \boldsymbol{P}_{2,2}\boldsymbol{\omega}\right) \tag{17}$$

where $\boldsymbol{P}_{2,1}$ and $\boldsymbol{P}_{2,2}$ are defined in (34) and found in (37). We emphasize to the reader that although the power system dynamics are nonlinear in nature, the control signals (and consequently the output of the ESSs) are derived using the linear approximated model in (10). However, in the numerical results in Section V, the performance of the LFO control scheme is evaluated by applying the controller of (17) to the nonlinear power system model of (1) and (2).

Even though the control scheme is dubbed *distributed*, it is observed that to calculate (17), the LFO controller requires the availability of the state information of all agents of the system. In this manner, a rich information sharing system is envisioned in the cyber–physical system where a communication network connects the different agents of the smart grid.

C. Steady-State Behavior

We define $\boldsymbol{x}^*$ and $\boldsymbol{y}^*$ as the steady-state values of $\boldsymbol{x}$ and $\boldsymbol{y}$ (where $\boldsymbol{y} = \boldsymbol{x} + \boldsymbol{A}^{-1}\boldsymbol{c}$), respectively. From (38), it can be deduced that $\boldsymbol{y}^* = \boldsymbol{0}$ as the eigenvalues of $\left(\boldsymbol{A} - \boldsymbol{L}\boldsymbol{R}^{-1}\boldsymbol{L}^T\boldsymbol{P}\right)$ lie in the left-hand complex plane. Thus, $\boldsymbol{x}^* = -\boldsymbol{A}^{-1}\boldsymbol{c}$. Given the structure of $\boldsymbol{A}$ in (15), then $\boldsymbol{A}^{-1} = \left[\begin{smallmatrix} \boldsymbol{\gamma}^{-1}\boldsymbol{D} & \boldsymbol{\gamma}^{-1}\boldsymbol{M} \\ \boldsymbol{I}_{N\times N} & \boldsymbol{0}_{N\times N} \end{smallmatrix}\right]$. As such, the steady-state value of $\boldsymbol{x}$ is expressed as

$$\begin{aligned} \boldsymbol{x}^* &= -\begin{bmatrix} \boldsymbol{D}\,\boldsymbol{\gamma}^{-1}\boldsymbol{M} \\ \boldsymbol{I} \quad \boldsymbol{0} \end{bmatrix} \times \begin{bmatrix} \boldsymbol{0} \\ \boldsymbol{M}^{-1}\boldsymbol{P}_m \end{bmatrix} \\ &= \begin{bmatrix} -\boldsymbol{\gamma}^{-1}\boldsymbol{P}_m \\ \boldsymbol{0} \end{bmatrix}. \end{aligned} \tag{18}$$

This implies $\boldsymbol{\delta}^* = -\boldsymbol{\gamma}^{-1}\boldsymbol{P}_m$ and $\boldsymbol{\omega}^* = \mathbf{0}$ (where $\boldsymbol{\delta}^*$ and $\boldsymbol{\omega}^*$ are the steady-state values of $\boldsymbol{\delta}$ and $\boldsymbol{\omega}$, respectively). Consequently, exponential speed synchronization is achieved by applying the LFO control scheme.

As a result of (17) and (18), the value of the control signal during steady state will be

$$\begin{aligned} \boldsymbol{u}^* &= -\boldsymbol{M}\boldsymbol{K}_{2,1}\left(\boldsymbol{\delta}^* + \boldsymbol{\gamma}^{-1}\boldsymbol{P}_m\right) \\ &= \mathbf{0}. \end{aligned} \tag{19}$$

That means the controller is expected to cease working after it stabilizes the power system. However, the values of $\boldsymbol{\delta}^*$ and $\boldsymbol{u}^*$ in (18) and (19) are a result of assuming the linearized swing equation model in (11). Actually, utilizing the nonlinear swing model of (4), the steady-state value of the control output will be found from

$$\begin{aligned} \dot{\boldsymbol{\omega}}^* &= -\boldsymbol{M}^{-1}\boldsymbol{D}\boldsymbol{\omega}^* + \boldsymbol{M}^{-1}\boldsymbol{P}_a + \boldsymbol{M}^{-1}\boldsymbol{u}^* \\ \mathbf{0} &= \mathbf{0} + \boldsymbol{M}^{-1}\boldsymbol{P}_a + \boldsymbol{M}^{-1}\boldsymbol{u}^*. \end{aligned} \tag{20}$$

In other words, $\boldsymbol{u}^* = -\boldsymbol{P}_a$. This result confirms that in order to keep the power system stable (i.e., $\boldsymbol{\omega} = \mathbf{0}$), the linear feedback controller has to compensate for any difference between the electrical and mechanical powers of the synchronous generators in the system, and this will stay the case until a governor control closes the gap between $P_{e,i}$ and $P_{m,i}$. Furthermore, using the value of $\boldsymbol{u}$ from (17) leads to

$$\boldsymbol{P}_a = \boldsymbol{M}\boldsymbol{R}_x^{-1}\boldsymbol{P}_{2,1}\left(\boldsymbol{\delta}^* + \boldsymbol{\gamma}^{-1}\boldsymbol{P}_m\right). \tag{21}$$

Solving for $\boldsymbol{\delta}^*$ yields

$$\boldsymbol{\delta}^* = \boldsymbol{P}_{2,1}^{-1}\boldsymbol{R}_x\boldsymbol{M}^{-1}\boldsymbol{P}_a - \boldsymbol{\gamma}^{-1}\boldsymbol{P}_m. \tag{22}$$

As such, if $\boldsymbol{P}_m = \boldsymbol{P}_e$ (as a result of an active governor control that compensates for the difference between $\boldsymbol{P}_m$ and $\boldsymbol{P}_e$), then $\boldsymbol{P}_a = \mathbf{0}$ and the value of $\boldsymbol{\delta}^*$ will be the same as to that found from the linearized model in (18).

D. Robustness Study

We investigate the robustness of the LFO controller in the presence of model errors and/or measurement uncertainties. Let $\hat{\omega}_i$ and $\hat{\delta}_i$ denote the (imprecise) estimates of the ω_i and δ_i, respectively. Furthermore, the uncertainty in the nonlinear component of the electromechanical dynamics is captured using $\hat{P}_{a,i}$. In this case, the relationships between the actual and estimated variables are represented as

$$\begin{aligned} \hat{\boldsymbol{\omega}} &= (\boldsymbol{I} + \boldsymbol{e}_\omega)\,\boldsymbol{\omega}, \quad \hat{\boldsymbol{\delta}} = (\boldsymbol{I} + \boldsymbol{e}_\delta)\,\boldsymbol{\delta} \\ \hat{\boldsymbol{P}}_a &= (\boldsymbol{I} + \boldsymbol{e}_{P_a})\,\boldsymbol{P}_a \end{aligned} \tag{23}$$

where $\boldsymbol{e}_\omega$, $\boldsymbol{e}_\delta$, and $\boldsymbol{e}_{P_a}$ are diagonal matrices that capture the degree of uncertainty in $\boldsymbol{\omega}$, $\boldsymbol{\delta}$, and $\boldsymbol{P}_a$, respectively. Furthermore, let $\tilde{\boldsymbol{A}} = \boldsymbol{A} - \boldsymbol{L}\boldsymbol{R}^{-1}\boldsymbol{L}^T\boldsymbol{P}$.

1) Model Error: In this case, we focus on the effect of model error and neglect measurement uncertainties; thus, we assume that $e_{\delta_i}, e_{\omega_i} \ll 1 \forall i \in \{1, \ldots, N\}$. Model uncertainty analysis results in an additional term called $\hat{f}_{\mathrm{NL}}(\boldsymbol{y})$ in (38); actually, $\hat{f}_{\mathrm{NL}}(\boldsymbol{y})$ is a nonlinear term that we will account for using Lyapunov redesign [37].

Consider a Lyapunov function V of the following form:

$$V(\boldsymbol{y}) = \boldsymbol{y}^T\boldsymbol{P}_v\boldsymbol{y} \tag{24}$$

where $\boldsymbol{P}_v$ is a $2N \times 2N$ positive definite matrix. Taking the time derivative of V gives

$$\begin{aligned} \dot{V}(\boldsymbol{y}) &= \dot{\boldsymbol{y}}^T\boldsymbol{P}_v\boldsymbol{y} + \boldsymbol{y}^T\boldsymbol{P}_v\dot{\boldsymbol{y}} \\ &= \left(\tilde{\boldsymbol{A}}\,\boldsymbol{y} + \hat{f}_{\mathrm{NL}}(\boldsymbol{y})\right)^T\boldsymbol{P}_v\boldsymbol{y} \\ &\quad + \boldsymbol{y}^T\boldsymbol{P}_v\left(\tilde{\boldsymbol{A}}\,\boldsymbol{y} + \hat{f}_{\mathrm{NL}}(\boldsymbol{y})\right) \\ &= \boldsymbol{y}^T(\tilde{\boldsymbol{A}}^T\boldsymbol{P}_v + \boldsymbol{P}_v\tilde{\boldsymbol{A}})\boldsymbol{y} + 2\hat{f}_{\mathrm{NL}}(\boldsymbol{y})\boldsymbol{P}_v\boldsymbol{y}. \end{aligned} \tag{25}$$

Let $\boldsymbol{Q}_v = -(\tilde{\boldsymbol{A}}^T\boldsymbol{P}_v + \boldsymbol{P}_v\tilde{\boldsymbol{A}})$, which can be shown to be positive definite given that $\tilde{\boldsymbol{A}}$ is Hurwitz. Moreover, we let $\boldsymbol{R}_v = 2\hat{f}_{\mathrm{NL}}(\boldsymbol{y})\boldsymbol{P}_v$ to give

$$\begin{aligned} \dot{V}(\boldsymbol{y}) &= -\boldsymbol{y}^T\boldsymbol{Q}_v\boldsymbol{y} + \boldsymbol{R}_v\boldsymbol{y} \\ &\leq -\lambda_{\min}(\boldsymbol{Q}_v)\|\boldsymbol{y}\|^2 + \|\boldsymbol{R}_v\|_\infty\|\boldsymbol{y}\| \\ &= -\lambda_{\min}(\boldsymbol{Q}_v)\left(\|\boldsymbol{y}\| - \frac{\|\boldsymbol{R}_v\|_\infty}{\lambda_{\min}(\boldsymbol{Q}_v)}\right)\|\boldsymbol{y}\|. \end{aligned} \tag{26}$$

Here, $\lambda_{\min}(\boldsymbol{Q}_v) > 0$ is the minimum eigenvalue of the positive definite matrix $\boldsymbol{Q}_v$, $\|\boldsymbol{y}\| \geq 0$ is the ℓ^2-norm of vector $\boldsymbol{y}$, and $\|\boldsymbol{R}_v\|_\infty > 0$ is the maximum absolute value of the elements in $\boldsymbol{R}_v$. Consequently, $\dot{V}(\boldsymbol{y}) < 0$ for $\|\boldsymbol{y}\| > \|\boldsymbol{R}_v\|_\infty/\lambda_{\min}(\boldsymbol{Q}_v)$.

As a result, an ultimate boundedness to a neighborhood that includes the origin is established in (26). This result means that the system state variables are able to converge toward the origin up to this neighborhood. Moreover, the neighborhood decreases in size for decreasing magnitudes of e_{P_i} and for increasing values of the minimum eigenvalue of $\boldsymbol{Q}_v$.

2) Measurement Uncertainty: In this case, we neglect model uncertainties and focus on the effects of measurement errors; thus, we assume $e_{P_i} \ll 1 \forall i \in \{1, \ldots, N\}$. The presence of measurement uncertainty affects the operation of the controller, and the value of the control signal becomes

$$\begin{aligned} \hat{\boldsymbol{u}} &= -\boldsymbol{M}\boldsymbol{R}_x^{-1}\left(\boldsymbol{P}_{2,1}\left(\hat{\boldsymbol{\delta}} + \boldsymbol{\gamma}^{-1}\boldsymbol{P}_m\right) + \boldsymbol{P}_{2,2}\hat{\boldsymbol{\omega}}\right) \\ &= \boldsymbol{u} + \boldsymbol{e}_u \end{aligned} \tag{27}$$

where $\boldsymbol{u}$ is found from (17), and $\boldsymbol{e}_u$ is the error in the control signal expressed as

$$\boldsymbol{e}_u = -\boldsymbol{M}\boldsymbol{R}_x^{-1}\left(\boldsymbol{P}_{2,1}\boldsymbol{e}_\delta\boldsymbol{\delta} + \boldsymbol{P}_{2,2}\boldsymbol{e}_\omega\boldsymbol{\omega}\right). \tag{28}$$

This error changes the dynamics of $\boldsymbol{y}$ in (38) as

$$\begin{aligned} \dot{\boldsymbol{y}} &= \tilde{\boldsymbol{A}}\boldsymbol{y} + \boldsymbol{M}^{-1}\begin{bmatrix}\mathbf{0} \\ \boldsymbol{e}_u\end{bmatrix} \\ &= \tilde{\boldsymbol{A}}\boldsymbol{y} - \begin{bmatrix}\mathbf{0} \\ \boldsymbol{R}_x^{-1}\left(\boldsymbol{P}_{2,1}\boldsymbol{e}_\delta\boldsymbol{\delta} + \boldsymbol{P}_{2,2}\boldsymbol{e}_\omega\boldsymbol{\omega}\right)\end{bmatrix} \\ &= \tilde{\boldsymbol{A}}\boldsymbol{y} + \boldsymbol{c}_y. \end{aligned} \tag{29}$$

TABLE I
FAULT TEST CASES

Case Study	Faulted Bus	Tripped Line
1	17	17–18
2	11	10–11
3	22	21–22
4	29	28–29

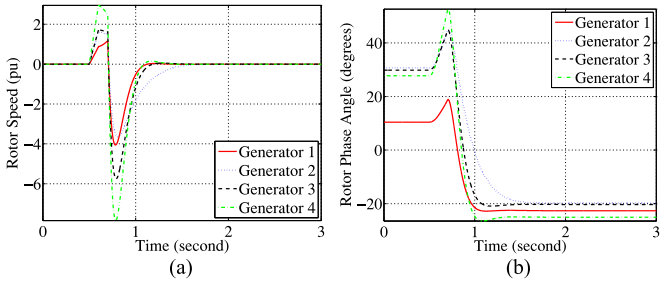

Fig. 2. Controller performance. (a) Rotor speed ω. (b) Rotor phase angle δ.

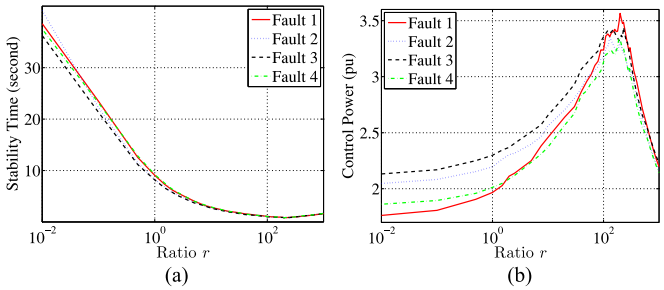

Fig. 3. Performance versus ratio r. (a) Stability time. (b) Control power.

If $\boldsymbol{R}_x^{-1}(\boldsymbol{P}_{2,1}\boldsymbol{e}_\delta\boldsymbol{\delta} + \boldsymbol{P}_{2,2}\boldsymbol{e}_\omega\boldsymbol{\omega})$ is approximated as a constant, then the estimation error affects the steady-state value of $\boldsymbol{y}$ by introducing a bias in $\boldsymbol{\omega}^*$ through $-\tilde{\boldsymbol{A}}^{-1}\boldsymbol{c}_y$.

Furthermore, consider a Lyapunov function of the form $V(\boldsymbol{y}) = \boldsymbol{y}^T\boldsymbol{P}_v\boldsymbol{y}$, then an analysis similar to that in (24)–(26) can be conducted for this case. Let $\boldsymbol{Q}_v = -(\tilde{\boldsymbol{A}}^T\boldsymbol{P}_v + \boldsymbol{P}_v\tilde{\boldsymbol{A}})$ and $\boldsymbol{R}_v = 2\boldsymbol{c}_y\boldsymbol{P}_v$, then

$$\dot{V}(\boldsymbol{y}) \leq -\lambda_{\min}(\boldsymbol{Q}_v)\left(\|\boldsymbol{y}\| - \frac{\|\boldsymbol{R}_v\|_\infty}{\lambda_{\min}(\boldsymbol{Q}_v)}\right)\|\boldsymbol{y}\|. \tag{30}$$

Thus, $\dot{V}(\boldsymbol{y}) < 0$ for $\|\boldsymbol{y}\| > \|\boldsymbol{R}_v\|_\infty/\lambda_{\min}(\boldsymbol{Q}_v)$. Consequently, an ultimate boundedness to a neighborhood that includes the origin is also established. Furthermore, the size of this neighborhood decreases for decreasing magnitudes of e_{δ_i} and e_{ω_i}.

V. Empirical Results and Discussion

We next numerically assess the performance of our proposed distributed LFO controller under ideal and nonideal conditions and compare it to prior art of Section III-C.

A. Simulation Environment

The New England 10-generator 39-bus test power system is considered. This test system has enough complexity to enable tractable analysis and meaningful insights. The values of M_i's and X'_{di}'s are found from [38] and [39] and the damping coefficients are set to 20 ms. Furthermore, Generator 10 (at Bus 39) in this system represents an equivalent "aggregate" generator modeling a large number of smaller generators.

Four case studies of symmetrical three-phase faults are considered in this paper, as shown in Table I. From $t = 0$ to $t = 0.5$ s, the power system is assumed to be running in normal state. Next, at $t = 0.5$ s, a three-phase fault occurs at the faulted bus. Then, at $t = 0.6$ s, the tripped line is removed to clear the fault. Finally, at $t = 0.7$ s, the stabilizing controller is activated on all generators (i.e., $t_0 = 0.7$ s).

Stability time of a generator is measured in this paper as $t_s - t_0$. In this case, t_s is the time after which the relative normalized rotor speed of the synchronous generator is restricted to the 0.8333% threshold, i.e., t_s is the time after which the actual rotor speed is limited to $\pm$ 0.5 Hz. In addition, the control power is calculated as the total external power that is injected and absorbed during the $[t_0, t_s]$ interval. Furthermore, Generator 10 is not included in the calculations given that it models a huge equivalent generator cluster.

The nonlinear model of (1) and (2) is used to simulate the power system; however, the linearized swing equation model of (11) and (12) is used to derive the value of the feedback control signal in (17). Let $\boldsymbol{R}_x$ in (16) be the identity matrix. Let also $\boldsymbol{Q}_x = r\boldsymbol{I}$, where $r > 0$ is a tunable design parameter that equals the ratio of the diagonal elements of $\boldsymbol{Q}_x$ and $\boldsymbol{R}_x$. Except in Fig. 3, a value of $r = 200$ is utilized in the following numerical results.

B. Performance of the LFO Controller

Fig. 2 displays the rotor phase angle and normalized speed of Generators 1–4 for Case Study 1 (i.e., a three-phase symmetrical fault at Bus 17). It is observed here that the rotor speed is quickly brought back to stability (i.e., $\lim_{t\to\infty}\omega_i(t) = 0$ is satisfied).

The performance of the controller versus the design parameter r is investigated in Fig. 3. It is shown that the lowest stability time for the four cases of fault is achieved when $r \approx 200$; however, the control power is greatest when $r \approx 200$. Results of this figure emphasize that r is a parameter that can be tailored to achieve specific stability time while meeting a constraint on control power.

C. Performance Under Practical Limitations

Before the sensor readings are sent over the communication channel to the LFO controllers, the measurements are sampled at a certain sampling period, termed as T_s. Higher values of T_s means that the sensors measure the system parameters less frequently and the controllers get less frequent updates about $\boldsymbol{x}$. The performance of the controller versus sampling time (T_s) is shown in Fig. 4. The LFO controller requires frequent system updates; otherwise, it cannot efficiently stabilize.

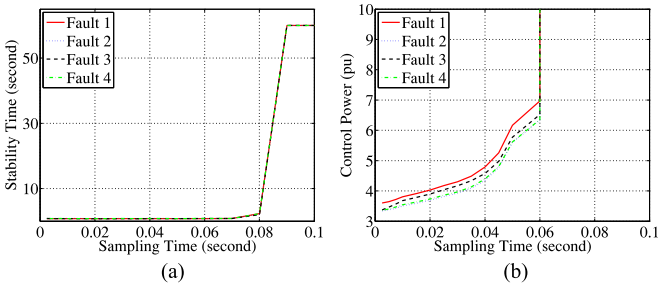

Fig. 4. Performance versus sampling time. (a) Stability time. (b) Control power.

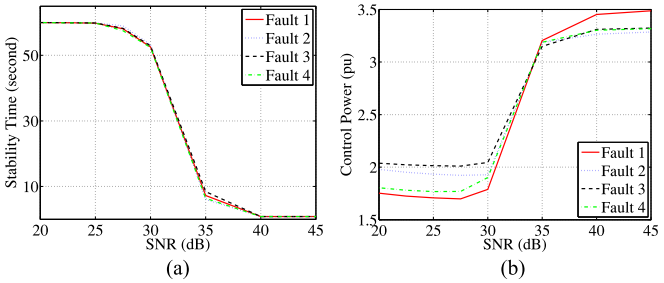

Fig. 5. Performance versus SNR. (a) Stability time. (b) Control power.

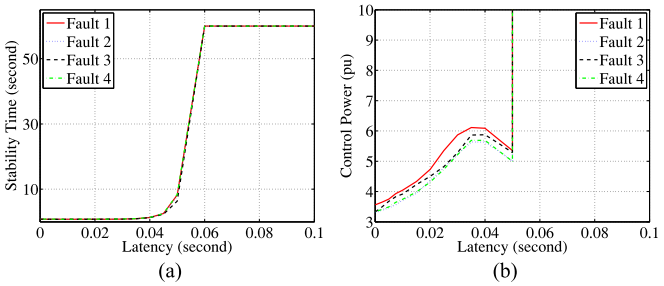

Fig. 6. Performance versus latency. (a) Stability time. (b) Control power.

Signal-to-noise ratio (SNR) is one metric of the quality of the received sensor readings at the LFO controller side; the lower the value of SNR, the lower the accuracy and fidelity of the received measurements. Fig. 5 displays the effect of SNR on the performance of the LFO controller. It is observed that the LFO controller requires a relatively high value of SNR in order to quickly stabilize the power system.

Communication latency occurs in the communication network of the smart grid due to many reasons, including sampling and quantization, encryption, transmission, channel propagation, and queueing delays. The effect of communication latency on the controller's performance is displayed in Fig. 6. Low latency values are important such that the LFO controller can efficiently stabilize the power system; this result aligns with the recommendations found in [40].

D. Performance Comparison and Discussion

The performance of the LFO control scheme is compared to that of the BESS-based control [7] (with storage capacity of 15% of system power), flocking control [8], CPI control [31] (with both α_c and $\beta_c = 0.25$), and PFL control [10] (with $\alpha = 0.5$) distributed schemes for the four cases of fault. The relationship between the average stability time (where $|\Delta\omega| \leq 0.00125$ p.u. is used for generator stability) and the control power of the different control schemes is shown in Fig. 7.

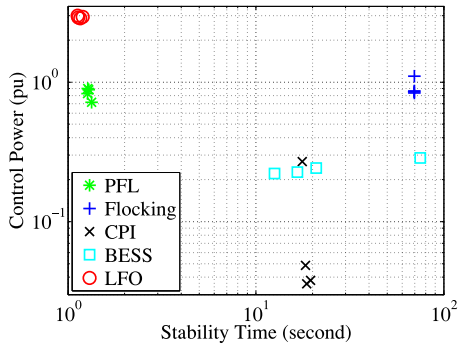

Fig. 7. Stability time versus control power performance comparison.

We assert that following are the attractive characteristics for a smart grid transient stability control paradigm.

1) Time criticality such that operation toward achieving transient stability is rapid to match the decreasing operational time scales in modern power systems.

2) Distributed nature to enable improved performance, scalability of communication, and resilience.

3) Simple and tractable design given that the distributed nature of control that requires implementation of control laws at each agent.

4) Tunability to provide a tradeoff between stability time and required control power.

As evident in Fig. 7, the proposed LFO controller aggressively restores transient stability. In fact, compared to the four other controllers, the LFO has the fastest stability time, which is critical for transient stability. However, it is also clear that this remarkable performance comes at a price of required control power. Although the PFL controller appears to provide an overall better tradeoff between stability time and control power, it cannot provide the most aggressive stabilization.

We are currently witnessing a shift in power system dynamics to significantly shorter time scales due to the increased penetration of distributed energy resources with low inertia. Moreover, the integration of cyber infrastructure shifts vulnerabilities to include the information infrastructure that can have profoundly negative consequences on operation. Thus, we assert that there is a growing need to achieve stability within much narrower time margins. Consequently, a controller for transient stability would be time critical and may be worth the additional power cost.

We assert that other advantages exist for the LFO controller that include linearity of control structure that allows for simpler implementation and analysis as well as tunability that enables balancing a tradeoff between control power and stability time. Such flexibility is not possible in all other techniques. Thus, the LFO controller provides an aggressive, yet simple, alternative to other recently proposed distributed control schemes. However,

the controller's limitations are in control power and performance in some nonideal environments.

Proper performance of this controller requires low latency, frequent, and high-integrity data of the system state information. Furthermore, the cost of utilizing this controller, measured in control power and number of ESSs, is higher. In summary, the investigated linear optimal control scheme provides an effective performance in comparison with other more complex nonlinear control approaches. Overall, we believe that the advantages of the LFO outweigh, for many operationally critical applications, the power efficiency of the PFL controller.

VI. Conclusion

The performance of a distributed linear quadratic optimal control paradigm for smart grid systems is investigated. Our framework leverages the connectivity of generator agents to obtain timely measurements for the actuation of fast-acting ESSs. We study the resilience provided by our control paradigm by applying it to the New England test power system. We also study the impact of practical issues including communication latency, sampling rate of sensors, and sensor SNR on controller performance.

Our investigation enables us to draw the following conclusions. In relation to other recently proposed distributed control schemes, the LFO controller provides the most aggressive alternative for transient stabilization as it can achieve stability fastest. In addition, LFO controller has a very simple structure in relation to recent work. Finally, the proposed distributed controller leverages the growing connectivity within the smart grid and is tunable. Thus, the proposed controller provides an excellent control strategy for time critical stability applications representing an excellent addition to the stability tools available to system operators.

Appendix
Mathematical Derivation

Let $\boldsymbol{y} = \boldsymbol{x} + \boldsymbol{A}^{-1}\boldsymbol{c}$, then the dynamics of the synchronous generators appears as

$$\dot{\boldsymbol{y}} = \boldsymbol{A}\boldsymbol{y} + \boldsymbol{L}\tilde{\boldsymbol{u}}. \tag{31}$$

Furthermore, an equivalent quadratic cost can be defined as [35]

$$J = \int_{t_0}^{\infty} \boldsymbol{y}(t)^T \boldsymbol{Q}\boldsymbol{y}(t) + \tilde{\boldsymbol{u}}(t)^T \boldsymbol{R}\tilde{\boldsymbol{u}}(t)\,\mathrm{d}t \tag{32}$$

where

$$\boldsymbol{Q} = \begin{bmatrix} \boldsymbol{0}_{N\times N} & \boldsymbol{0}_{N\times N} \\ \boldsymbol{0}_{N\times N} & \boldsymbol{Q}_x \end{bmatrix}, \boldsymbol{R} = \begin{bmatrix} \boldsymbol{I}_{N\times N} & \boldsymbol{0}_{N\times N} \\ \boldsymbol{0}_{N\times N} & \boldsymbol{R}_x \end{bmatrix}. \tag{33}$$

In addition, we define

$$\boldsymbol{K} = \begin{bmatrix} \boldsymbol{K}_{1,1} & \boldsymbol{K}_{1,2} \\ \boldsymbol{K}_{2,1} & \boldsymbol{K}_{2,2} \end{bmatrix}, \boldsymbol{P} = \begin{bmatrix} \boldsymbol{P}_{1,1} & \boldsymbol{P}_{1,2} \\ \boldsymbol{P}_{2,1} & \boldsymbol{P}_{2,2} \end{bmatrix} \tag{34}$$

where $\boldsymbol{K}_{1,1}, \ldots, \boldsymbol{K}_{2,2}$ and $\boldsymbol{P}_{1,1}, \ldots, \boldsymbol{P}_{2,2}$ are $N \times N$ matrices, and $\boldsymbol{K}$ and $\boldsymbol{P}$ are matrices that need to be found during the optimization process.

The linear feedback control that minimizes the value of J can be expressed as $\tilde{\boldsymbol{u}} = -\boldsymbol{K}\boldsymbol{y}$, which leads to

$$\dot{\boldsymbol{y}} = (\boldsymbol{A} - \boldsymbol{L}\boldsymbol{K})\,\boldsymbol{y}. \tag{35}$$

The solution of which is given by $\boldsymbol{y}(t) = e^{(\boldsymbol{A}-\boldsymbol{L}\boldsymbol{K})t}\,\boldsymbol{y}_0$, where $\boldsymbol{y}_0$ is the value of $\boldsymbol{y}(t)$ at t_0. Furthermore, if linear quadratic optimal control is used to solve (32), then the LFO control matrix is expressed as [41], [42]

$$\boldsymbol{K} = \boldsymbol{R}^{-1}\boldsymbol{L}^T\boldsymbol{P} \tag{36}$$

where $\boldsymbol{P} \in \mathbb{R}^{2N\times 2N}$ is the unique positive semidefinite solution to the following algebraic Riccati equation [41], [42]:

$$\boldsymbol{0} = \boldsymbol{A}^T\boldsymbol{P} + \boldsymbol{P}\boldsymbol{A} + \boldsymbol{Q} - \boldsymbol{P}\boldsymbol{L}\boldsymbol{R}^{-1}\boldsymbol{L}\boldsymbol{P}. \tag{37}$$

The above Riccati equation can be solved using matrix factorization or by dynamic programming. Consequently,

$$\dot{\boldsymbol{y}} = \left(\boldsymbol{A} - \boldsymbol{L}\boldsymbol{R}^{-1}\boldsymbol{L}^T\boldsymbol{P}\right)\boldsymbol{y}. \tag{38}$$

Utilizing the values of $\boldsymbol{R}$, $\boldsymbol{L}$, and $\boldsymbol{P}$, the value of the feedback gain is

$$\begin{aligned} \boldsymbol{K} &= \begin{bmatrix} \boldsymbol{I} & \boldsymbol{0} \\ \boldsymbol{0} & \boldsymbol{R}_x^{-1} \end{bmatrix} \begin{bmatrix} \boldsymbol{0} & \boldsymbol{0} \\ \boldsymbol{0} & \boldsymbol{I} \end{bmatrix} \begin{bmatrix} \boldsymbol{P}_{1,1} & \boldsymbol{P}_{1,2} \\ \boldsymbol{P}_{2,1} & \boldsymbol{P}_{2,2} \end{bmatrix} \\ &= \begin{bmatrix} \boldsymbol{0} & \boldsymbol{0} \\ \boldsymbol{R}_x^{-1}\boldsymbol{P}_{2,1} & \boldsymbol{R}_x^{-1}\boldsymbol{P}_{2,2} \end{bmatrix}. \end{aligned} \tag{39}$$

In this case, both $\boldsymbol{K}_{1,1}$ and $\boldsymbol{K}_{1,2}$ are equal to $\boldsymbol{0}$, $\boldsymbol{K}_{2,1} = \boldsymbol{R}_x^{-1}\boldsymbol{P}_{2,1}$, and $\boldsymbol{K}_{2,2} = \boldsymbol{R}_x^{-1}\boldsymbol{P}_{2,2}$. Once the elements of $\boldsymbol{P}$ are determined, the value of $\boldsymbol{K}$ is obtained from (39). This implies that $\tilde{\boldsymbol{u}} = -\boldsymbol{K}\boldsymbol{y} = -\boldsymbol{K}\left(\boldsymbol{x} + \boldsymbol{A}^{-1}\boldsymbol{c}\right)$ can be calculated as

$$\tilde{\boldsymbol{u}} = -\begin{bmatrix} \boldsymbol{0}_{N\times 1} \\ \boldsymbol{K}_{2,1}\left(\boldsymbol{\delta} + \boldsymbol{\gamma}^{-1}\boldsymbol{P}_m\right) + \boldsymbol{K}_{2,2}\boldsymbol{\omega} \end{bmatrix}. \tag{40}$$

Consequently, the value of the LFO control signal is found from $\boldsymbol{M}\hat{\boldsymbol{u}}$, where $\hat{\boldsymbol{u}}$ is the lower half of $\tilde{\boldsymbol{u}}$. In other words, $\boldsymbol{u} = -\boldsymbol{M}\left(\boldsymbol{K}_{2,1}\left(\boldsymbol{\delta} + \boldsymbol{\gamma}^{-1}\boldsymbol{P}_m\right) + \boldsymbol{K}_{2,2}\boldsymbol{\omega}\right)$.

References

[1] R. Deng, R. Lu, G. Xiao, and J. Chen, "Fast distributed demand response with spatially-and temporally-coupled constraints in smart grid," *IEEE Trans. Ind. Informat.*, vol. 11, no. 3, pp. 1551–1606, Dec. 2015.

[2] R. Deng, Z. Yang, M.-Y. Chow, and J. Chen, "A survey on demand response in smart grids: Mathematical models and approaches," *IEEE Trans. Ind. Informat.*, vol. 11, no. 3, pp. 570–582, Jun. 2015.

[3] P. Parikh, T. Sidhu, and A. Shami, "A comprehensive investigation of wireless LAN for IEC 61850-based smart distribution substation applications," *IEEE Trans. Ind. Informat.*, vol. 9, no. 3, pp. 1466–1476, Aug. 2013.

[4] H. Tung "The generic design of a high-traffic advanced metering infrastructure using ZigBee," *IEEE Trans. Ind. Informat.*, vol. 10, no. 1, pp. 836–844, Feb. 2014.

[5] S. Das and T. Singh Sidhu, "Application of compressive sampling in synchrophasor data communication in WAMS," *IEEE Trans. Ind. Informat.*, vol. 10, no. 1, pp. 450–460, Feb. 2014.

[6] V. Güngör "Smart grid technologies: Communication technologies and standards," *IEEE Trans. Ind. Informat.*, vol. 7, no. 4, pp. 529–539, Nov. 2011.

[7] P. Mercier, R. Cherkaoui, and A. Oudalov, "Optimizing a battery energy storage system for frequency control application in an isolated power system," *IEEE Trans. Power Syst.*, vol. 24, no. 3, pp. 1469–1477, Aug. 2009.

[8] J. Wei, D. Kundur, T. Zourntos, and K. Butler-Purry, "A flocking-based paradigm for hierarchical cyber-physical smart grid modeling and control," *IEEE Trans. Smart Grid*, vol. 5, no. 6, pp. 2687–2700, Nov. 2014.
[9] E. Hammad, A. Farraj, and D. Kundur, "A resilient feedback linearization control scheme for smart grids under cyber-physical disturbances," in *Proc. IEEE PES Conf. Innovative Smart Grid Technol.*, Feb. 2015, pp. 1–5.
[10] A. Farraj, E. Hammad, and D. Kundur, "A cyber-enabled stabilizing control scheme for resilient smart grid systems," *IEEE Trans. Smart Grid*, vol. 7, no. 4, pp. 1856–1865, Jul. 2016.
[11] J. Liu, W. Luo, X. Yang, and L. Wu, "Robust model-based fault diagnosis for PEM fuel cell air-feed system," *IEEE Trans. Ind. Electron.*, vol. 63, no. 5, pp. 3261–3270, May 2016.
[12] J. Liu, S. Laghrouche, and M. Wack, "Observer-based higher order sliding mode control of power factor in three-phase ac/dc converter for hybrid electric vehicle applications," *Int. J. Control*, vol. 87, no. 6, pp. 1117–1130, 2014.
[13] L. Wu, W. X. Zheng, and H. Gao, "Dissipativity-based sliding mode control of switched stochastic systems," *IEEE Trans. Automat. Control*, vol. 58, no. 3, pp. 785–791, Mar. 2013.
[14] A. Farraj, E. Hammad, A. AL Daoud, and D. Kundur, "A game-theoretic control approach to mitigate cyber switching attacks in smart grid systems," in *Proc. IEEE Int. Conf. Smart Grid Commun.*, Nov. 2014, pp. 958–963.
[15] A. Farraj, E. Hammad, A. AL Daoud, and D. Kundur, "A game-theoretic analysis of cyber switching attacks and mitigation in smart grid systems," *IEEE Trans. Smart Grid*, vol. 7, no. 4, pp. 1846–1855, Jul. 2016.
[16] F. Lin, *Robust Control Design: An Optimal Control Approach*. Hoboken, NJ, USA: Wiley, 2007.
[17] P. Kundur "Definition and classification of power system stability IEEE/CIGRE joint task force on stability terms and definitions," *IEEE Trans. Power Syst.*, vol. 19, no. 3, pp. 1387–1401, Aug. 2004.
[18] J. Machowski, J. Bialek, and J. Bumby, *Power System Dynamics: Stability and Control*, 2nd ed. Hoboken, NJ, USA: Wiley, 2008.
[19] N. Hingorani, "Flexible AC transmission," *IEEE Spectr.*, vol. 30, no. 4, pp. 40–45, Apr. 1993.
[20] O. Elgerd, "Control of electric power systems," *IEEE Control Syst. Mag.*, vol. 1, no. 2, pp. 4–16, Jun. 1981.
[21] P. Kundur, *Power System Stability and Control (EPRI Power System Engineering Series)*. New York, NY, USA: McGraw-Hill, 1994.
[22] P. Anderson and A. Fouad, *Power System Control and Stability (IEEE Power Systems Engineering Series)*. Piscataway, NJ, USA: IEEE Press, 1994.
[23] P. Sauer and M. Pai, *Power System Dynamics and Stability*. Englewood Cliffs, NJ, USA: Prentice-Hall, 1998.
[24] F. Dörfler and F. Bullo, "Kron reduction of graphs with applications to electrical networks," *IEEE Trans. Circuits Syst. I, Reg. Papers*, vol. 60, no. 1, pp. 150–163, Jan. 2013.
[25] A. Bergen and V. Vittal, *Power Systems Analysis*, 2nd ed. Englewood Cliffs, NJ, USA: Prentice-Hall, 2000.
[26] W. Li, M. Ferdowsi, M. Stevic, A. Monti, and F. Ponci, "Cosimulation for smart grid communications," *IEEE Trans. Ind. Informat.*, vol. 10, no. 4, pp. 2374–2384, Nov. 2014.
[27] A. Sabbah, A. El-Mougy, and M. Ibnkahla, "A survey of networking challenges and routing protocols in smart grids," *IEEE Trans. Ind. Informat.*, vol. 10, no. 1, pp. 210–221, Feb. 2014.
[28] C. Reynolds, "Flocks, herds, and schools: A distributed behavioral model," in *Proc. 14th Annul. Conf. Comput. Graph. Interactive Techn.*, Jul. 1987, vol. 21, pp. 25–34.
[29] R. Olfati-Saber, "Flocking for multi-agent dynamic systems: Algorithms and theory," *IEEE Trans. Automat. Control*, vol. 51, no. 3, pp. 401–420, Mar. 2006.
[30] R. Olfati-Saber, J. A. Fax, and R. Murray, "Consensus and cooperation in networked multi-agent systems," *Proc. IEEE*, vol. 95, no. 1, pp. 215–233, Jan. 2007.
[31] M. Andreasson, D. Dimarogonas, H. Sandberg, and K. Johansson, "Distributed control of networked dynamical systems: Static feedback and integral action and consensus," *IEEE Trans. Automat. Control*, vol. 59, no. 7, pp. 1750–1764, Jul. 2014.
[32] A. Farraj, E. Hammad, and D. Kundur, "A cyber-enabled stabilizing controller for resilient smart grid systems," in *Proc. IEEE PES Conf. Innovative Smart Grid Technol.*, Feb. 2015, pp. 1–5.
[33] K. Purchala, L. Meeus, D. Van Dommelen, and R. Belmans, "Usefulness of DC power flow for active power flow analysis," in *Proc. IEEE Power Eng. Soc. Gen. Meeting*, Jun. 2005, pp. 454–459.
[34] E. Sjödin, "The price of synchrony: Evaluating transient power losses in renewable energy integrated power networks," *Master's thesis, KTH School Elect. Eng., Stockholm, Sweden*, Aug. 2013.
[35] A. Farraj, E. Hammad, and D. Kundur, "On using distributed energy resources to reshape the dynamics of power systems during transients," in *Proc. IEEE Int. Conf. Smart Grid Commun.*, Nov. 2015, pp. 756–761.
[36] W. Wonham, *Linear Multivariable Control: A Geometric Approach*. New York, NY, USA: Springer-Verlag, 1985.
[37] H. Khalil, *Nonlinear Systems*, 3rd ed. Englewood Cliffs, NJ, USA: Prentice-Hall, 2002.
[38] T. Athay, R. Podmore, and S. Virmani, "A practical method for the direct analysis of transient stability," *IEEE Trans. Power App. Syst.*, vol. PAS-98, no. 2, pp. 573–584, Mar./Apr. 1979.
[39] B. Pal and B. Chaudhuri, *Robust Control in Power Systems (Power Electronics and Power Systems Series)*. New York, NY, USA: Springer, 2006.
[40] A. Phadke and J. Thorp, "Communication needs for wide area measurement applications," in *Proc. Int. Conf. Crit. Infrastruct.*, Sep. 2010, pp. 1–7.
[41] H. Kwakernaak and R. Sivan, *Linear Optimal Control Systems*. Hoboken, NJ, USA: Wiley, 1972.
[42] F. Lewis and V. Syrmos, *Optimal Control*. Hoboken, NJ, USA: Wiley, 1995.

Authors' photographs and biographies not available at the time of publication.